Engineering Structures 206 (2020) 110050

Contents lists available at ScienceDirect

Engineering Structures

journal homepage: www.elsevier.com/locate/engstruct

Cost-benefit analysis of traditional seismic retrofitting strategies integrated in the renovation of stone masonry buildings

Rui Maio[a,*], João M.C. Estêvão[b], Tiago Miguel Ferreira[c], Romeu Vicente[a]

[a] Aveiro Research Centre of Risks and Sustainability in Construction (RISCO), Department of Civil Engineering, University of Aveiro, Portugal
[b] Department of Civil Engineering, University of Algarve, Portugal
[c] Institute for Science and Innovation for Bio-Sustainability (IB-S), Department of Civil Engineering, University of Minho, Portugal

ARTICLE INFO

Keywords:
Cost-benefit analysis
Seismic retrofitting
Stone masonry buildings
Nonlinear static analyses
Macroelement approach
N2 method
Fragility curves
Loss estimation
HAZUS methodology

ABSTRACT

This study discusses the cost-benefit analysis resulting from the application of traditional seismic retrofitting strategies on four case studies considered representative of both rural and urban stone masonry building stock of Faial Island, in Azores (Portugal). The seismic performance-based assessment was carried out by applying the N2 Method procedure, and the global seismic capacity of each case study estimated by using a three-dimensional model based on the macroelement approach, which combines both the in-plane and out-of-plane response of masonry buildings, to perform nonlinear static analyses. Fragility and loss estimation was evaluated according to the HAZUS methodology. In general terms, the cost-benefit analysis has demonstrated that the studied retrofitting strategies are indeed capable of reducing substantially the seismic vulnerability of the considered case studies, and also that they represent, in fact, a limited amount of the total replacement cost, not compromising, therefore, their economic viability.

1. Introduction

The recent upsurge on the revitalisation of historical centres in Portugal, is contributing to the mischaracterisation phenomenon of urban cultural heritage (UCH) assets, as traditional construction techniques and materials are massively being replaced by modern solutions, totally disrupting the aesthetic value of existing assets, and often jeopardising the seismic vulnerability of such assets [1]. One of the preferred arguments used to underpin the phenomenon of both architectural and constructive mischaracterisation is that, allegedly, structural renovation works compliant with existing materials and traditional building techniques are not viable from the economic viewpoint. Another often cited argument is that such traditional materials and building techniques do not comply with the regulatory requirements in force in terms of seismic performance.

Hence, and as a follow-up of the research published by Maio et al. [1], the current study aims not only at investigating the authenticity of the arguments mentioned above but also to demystify the generalised idea that traditional strategies for the seismic retrofitting of UCH assets have a significant impact over the total renovation cost. In literature, the term “traditional techniques” usually refers to enhancing measures of the buildings’ structural integrity/stability by using compatible and local materials such as earth and wood, and solutions as ring beams, wooden ties interconnecting parallel walls, corner keys, or the addition of buttresses, for example. However, “traditional” has in this study an additional meaning, in the sense that these strategies are quite common and have been widely applied in the framework of the reconstruction process of Faial island (in Azores, Portugal), after the 1998 Azores earthquake [2]. The validation of the former hypotheses is going to be investigated by assessing the Cost-Benefit Analysis (CBA) of two of these strategies.

One of the first cost-benefit models for the seismic retrofitting of buildings was issued by the Federal Emergency Management Agency in 1994 [3,4], which encouraged the development of several studies in this topic ever since [5,6]. In the past few years, several compelling studies within this particular research field have been published, focusing either on residential [7,8] or public-school buildings [9,10]. It is worth noting that despite being widely acknowledged worldwide as a significant decision-supporting tool commonly used for evaluating the efficiency of projects, CBA does not provide an absolute answer about whether or not to undertake the seismic retrofitting of a given asset. This because the decision-making process usually depends on many factors beyond the boundaries of benefit-cost analysis, such as the definition of life safety and post-earthquake performance levels [3]. Notwithstanding these limitations, this study aims at investigating the referred hypotheses associated with the mischaracterisation

* Corresponding author at: Campus Universitário de Santiago, 3810-193 Aveiro, Portugal.
E-mail address: ruiamaio@ua.pt (R. Maio).

https://doi.org/10.1016/j.engstruct.2019.110050
Received 28 May 2019; Received in revised form 14 October 2019; Accepted 5 December 2019

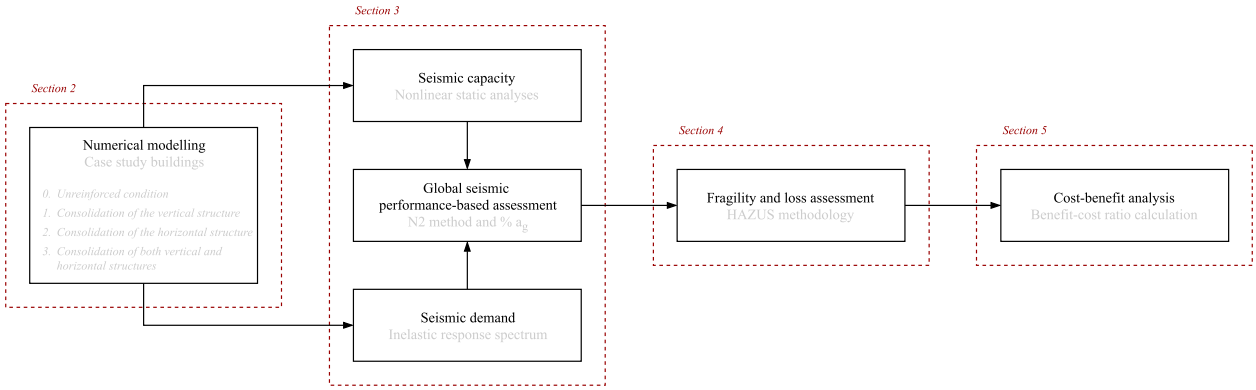

Fig. 1. Outline of the CBA model developed for the estimation of the cost-benefit of applying traditional seismic retrofitting strategies integrated in the renovation of UCH assets, agreeing with the outline of the paper.

phenomenon witnessed in many historical centres in Portugal, which causes and consequences, have been identified and discussed in [1].

The CBA model developed in this paper, outlined in Fig. 1, is expected to be a useful tool to support the decision-making process of all the stakeholders involved in the seismic renovation of UCH assets in Portugal.

Even though there are numerous techniques available in literature for the seismic retrofitting of traditional stone masonry structures, as demonstrated by Bento et al. [11], Costa and Arêde [12], Branco and Guerreiro [13], or Scotta et al. [14], in this study, focus will be given to traditional retrofitting techniques, which has been addressed for example in Diz et al. [15], Moreira [16], Maio et al. [17], or Ortega [18]. From these, the authors will only consider two of the most widely applied retrofitting solutions that were adopted by the Regional Government of Azores in the framework of the reconstruction process of Faial Island after the 1998 earthquake: the consolidation of the vertical and horizontal structures (full description follows in Section 2.2). The mean costs associated with these seismic retrofitting techniques were presented in [1], after a careful examination of the renovation cost records available in the database generated at the time of the referred reconstruction process of Faial Island.

2. Case studies

In this paper, the CBA model is going to be applied to a total of four case studies, taken, after Costa [19] and Maio et al. [1], as representative of both rural and urban traditional stone masonry typologies of Faial Island. The information available of these case studies included technical drawings, detailed documentation and photographic survey not only of the main structural features but also of the extent of damage observed in the aftermath of the 1998 Azores earthquake [2]. It also included both renovation and seismic retrofitting design projects, which supported the formulation of the retrofitting strategies herein adopted.

2.1. Geometry and building typology

As demonstrated in Fig. 2, these case studies (from A to D) present a quite regular plan which is kept consistent in height, with gross floor area (GFA) of 73, 129, 256 and 714 m^2, respectively. When comparing the main elevations of rural (A and B) and urban (C and D) typologies in Fig. 2, it is furthermore evident that urban typologies are adorned with several architectural features that highlight the grandness of these assets, such as the presence of ashlar stone masonry quoins, balconies, parapets, gable fronted dormers, among other decorative features.

If exclusively focusing on the characteristics of the elements of the vertical structural, these typologies fundamentally differ on the type and quality of the masonry fabric used for load-bearing walls, which was highly reliant on the wealth of their original owners and the location of the building. According to Costa [19], the most common stones used in the construction of Faial Island masonry building stock were basalt, cinerite, andesite, trachyte and volcanic tuff. The two rural typologies herein considered were built with double-leaf masonry walls resorting to stones slightly larger than half the wall width, being the gap between rocks filled with rubble, mud and lime mortar. The rendering of the external walls is variable, being the mixture of clay and lime, wherein 2.0 cm thick, over which a fine lime and sand mortar is applied, the most common rendering solution. Urban typologies instead are built with regular-sized stones or “blocks”. As demonstrated in Fig. 2, there are also a few walls made of concrete blocks (highlighted in light grey), such as those associated with the extension of building A, for example. The foundations are believed to be made of the same stone of masonry used for external walls but slightly wider and with a depth of at least 1.0 m, depending on the number of storeys of the building [19].

In what concerns to the horizontal structure, while the ground floor has a screed finishing, upper floors are composed of timber planks supported by timber joists, which are in turn supported on load-bearing walls. The roof structure is made of traditional timber trusses of two hip rafters, forming in the particular case of building D an additional story by taking advantage of the attic and four gable dormers. Even though gable dormers are a prominent feature of the Azorean architecture, these elements were disregarded in the numerical models considering the modelling limitations of the software code used in the case of very complex roof systems. Timber staircases provide access between storeys. Again, given the modelling constraints of the software code used, and also the insignificant influence of such lightweight and low stiffness elements over the global response of the building, when compared to load-bearing masonry walls, timber staircases were not considered in the numerical models.

2.2. Numerical models

In this study, a three-dimensional macroelement model developed by Pantò et al. [20] and compatible with the software code 3D-Macro® [21] was used. It includes both rocking and diagonal shear cracking mechanisms in the combined response (in-plane and out-of-plane) of masonry structures. The resulting numerical models are illustrated in Fig. 3. It is worth referring that a more refined mesh was used to better approximate the response of these models to the real behaviour of the respective case studies. However, as this measure might involve a substantial increase in the number of the degrees of freedom, the search for a plausible compromise between computation time and reliability of results is inevitable. Hence, the maximum dimension of masonry panels was set equal to 1.0 m.

In the software code 3D-Macro® [21], masonry panels are defined

Fig. 2. Overview of the geometry and building typology of each case study (from A to D): ground floor plans and the respective main façade elevations. Please note that traditional stone masonry elements are coloured in grey, while masonry brick blocks are coloured in light grey. Moreover, the reference axes (X and Y) considered throughout the paper to each model are identified in the respective ground floor plans.

by the following mechanical properties: elastic modulus (E); shear modulus (G); specific weight (w), compressive strength (f_m), shear strength (τ_0), and tensile strength (f_{tm}). The values of these properties, which were adopted for similar masonry typologies from the Italian Building Code [22], hereinafter referred to as NTC, are going to be presented in the next subsections for each retrofitting condition considered. Horizontal diaphragms (floor and roof elements) were modelled as rectangular diaphragms elastically deformable considering orthotropic slab elements, which are characterised by an equivalent thickness, s, Elastic moduli, $E_{1,eq}$ and $E_{2,eq}$, adopted respectively in the orthogonal and perpendicular direction of the floor warping, and an equivalent shear modulus, G_{eq}. The values of the Elastic moduli $E_{1,eq}$ and $E_{2,eq}$, were determined as a function of the geometry of the cross-section and the elasticity of timber planks and beams. Architrave elements (or lintels) were modelled as timber beams with a linear-elastic response, considering a Poisson's coefficient (υ) equal to 0.2. In this study, all timber elements were defined for the Azorean cryptomeria class, considering a mean elasticity modulus is equal to 3.9 GPa and specific weight of 2.6 kN m^{-3}. Gravity loads (G_k) equal to 1.0 kN m^{-2} were assumed to all horizontal diaphragms, while live loads (Q_k) were taken equal to 2.0 and 0.5 kN m^{-2}, respectively in the case of floor and roof elements. Finally, the interaction between the foundations and the underlying soil was disregarded in this study.

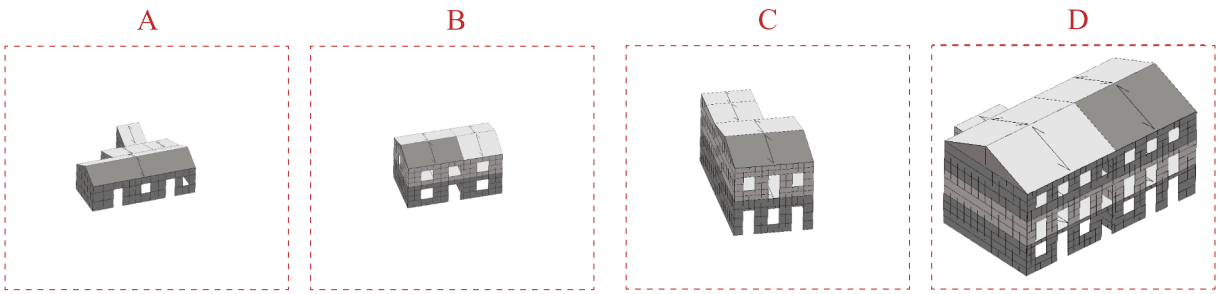

Fig. 3. Overview of the three-dimensional model of each model (A to D), developed by using the 3D-Macro® software code. Please note that the control node considered for each model was assigned at the centre of rigidity of the floor elements, highlighted in dark grey. The geometry of macroelements was limited to a maximum dimension of 1.0 m to have a more refined mesh and subsequently, a less conservative model.

Table 1
Mechanical properties of masonry walls assumed for the unreinforced condition. *[1]Please note that a cracked stiffness condition for masonry panels was considered, and for this reason, the elastic properties' values given below are already halved, according to the recommendation of the EN 1998-1 [26]. *[2]These values are already divided by a confidence factor, CF, equal to 1.35, which corresponds to a knowledge level, KL1 [23], adopted from Table C8A.2.1 of [22].

Masonry type	Building typology	E*[1] [MPa]	G*[1] [MPa]	w [kNm^{-3}]	f_m*[2] [Ncm^{-2}]	f_{tm}*[2] [Ncm^{-2}]	τ_0*[2] [Ncm^{-2}]
Stone	Rural	435	145	19	74.1	3.7	1.5
	Urban	615	205	20	148.1	7.4	2.6
Concrete blocks	Rural/Urban	700	175	12	111.1	5.6	7.0

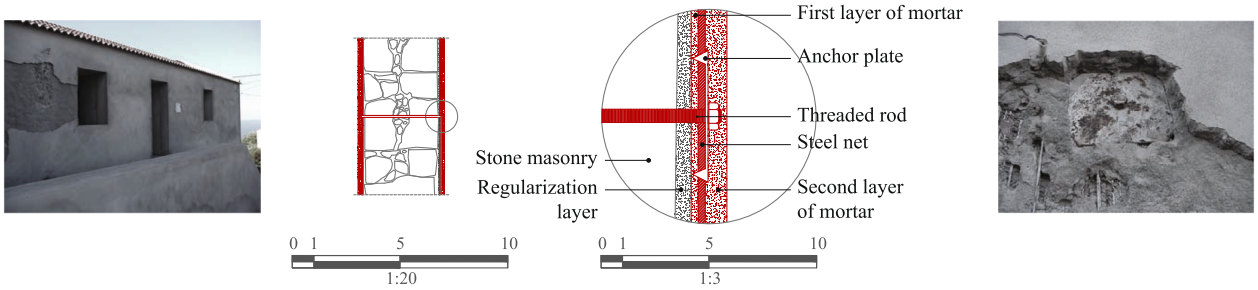

Fig. 4. Consolidation of the vertical structure (1) with a traditional reinforced render system.

Table 2
Masonry corrective coefficients considered for the consolidation of the vertical structure (1), assigned according to the recommendations of the NTC [22].

Corrective coefficient	E	G	f_m	τ_0
Transversal connectors	1.00	1.00	1.50	1.50
Mortar injections	2.00	2.00	2.00	2.00

2.2.1. Unreinforced model (0)

The values assigned to mechanical properties of masonry panels presented in Table 1, were adopted from the NTC [22] for "masonry in disorganised stones" and "dressed rectangular stone masonry" masonry typologies, respectively in the case of rural (buildings A and B) and urban (buildings C and D) building typologies. However, and despite the values of elastic properties are in line with the upper limit values proposed by Costa [19], for example, a knowledge level KL1 was considered [23]. The equivalent shear modulus of horizontal diaphragms, G_{eq}, was assigned equal to 6.8 MPa, according to the guidelines published by the NZSEE (New Zealand's Society of Earthquake Engineering) [24], after ASCE [25], considering a straight single sheathing timber floor typology in a poor rating condition. The equivalent thickness of horizontal diaphragms, s, was considered equal to 2.5 cm. The tensile strength of the masonry panels, f_{tm}, was assumed equal to 5% of the compressive strength value, f_m.

2.2.2. Consolidation of the vertical structure (1)

The first retrofitting strategy considered is the consolidation of the vertical structure, ensured by the application of the reinforced render system specified by Costa [19], on both sides of the external stone masonry walls, as illustrated in Fig. 4. The application of this reinforced render system is divided into three phases. A first layer of filling mortar in the proportion of 1:3 (local sand extracted from Fajã Beach: Portland cement: water) is applied for voids and surface regularisation. Then, a 0.5 mm thick welded and galvanised steel net made of S275 steel and 10.0 mm spaced ribs is installed and fixed on both sides of the masonry wall through a system composed of M20 galvanised screws, Φ20 galvanised steel threaded rods, and 4.0 mm thick anchor plates (20.0 × 20.0 mm wide and spaced each 1.5 m). Finally, a 3.0 cm thick second layer of fine sand-blasted finishing mortar is applied [19].

The consolidation of the vertical structure was simulated in 3D-Macro® by improving the mechanical properties of the masonry according to a set of corrective coefficients suggested by the NTC [22], which are given in Table 2. These coefficients were multiplied by the values assigned to the unreinforced condition (0), presented in the previous Table 1. In this case, it was considered a stiffness reduction of 25% of the initial (uncracked) value. As for the tensile strength provided by the reinforced render system applied to external stone masonry walls, f_{tm}, a value of 126.6 N cm^{-2}, proposed by Braga and EstêVão [27] for a similar cement-based render, was considered. This value was then divided by a confidence factor, CF, equal to 1.35, which corresponds to a knowledge level KL1, again following the recommendations of the NP EN 1998-3 [23]. In the case of concrete blocks, f_{tm} was assumed equal to 5% of the compressive strength value, f_m.

2.2.3. Consolidation of the horizontal structure (2)

The second retrofitting strategy consisted on the consolidation of the horizontal structure (improving the so-called box-behaviour), which comprised not only the improvement of the connections between the horizontal and the vertical structure, but also the in-plane stiffness of the original diaphragms. As demonstrated in Fig. 5 (a), this was made possible by installing a full-length angle bracket system connecting timber beams to external walls and by adding a new layer of timber sheathing, laid perpendicular and adequately nailed to the original timber sheathing.

Additionally, in Fig. 5 (b), 7.5 cm thick diagonal timber braces between timber beams at both floor and roof levels were installed and anchored through a system composed of Φ10 galvanised steel threaded rods and 3.0 mm thick galvanised steel angle brackets. Furthermore, an effort was made to keep and restore the original timber elements as much as possible, rather than replacing the whole timber structure by a new one.

2.2.4. Consolidation of both vertical and horizontal structure (3)

Finally, a third strategy was considered, which consisted of the

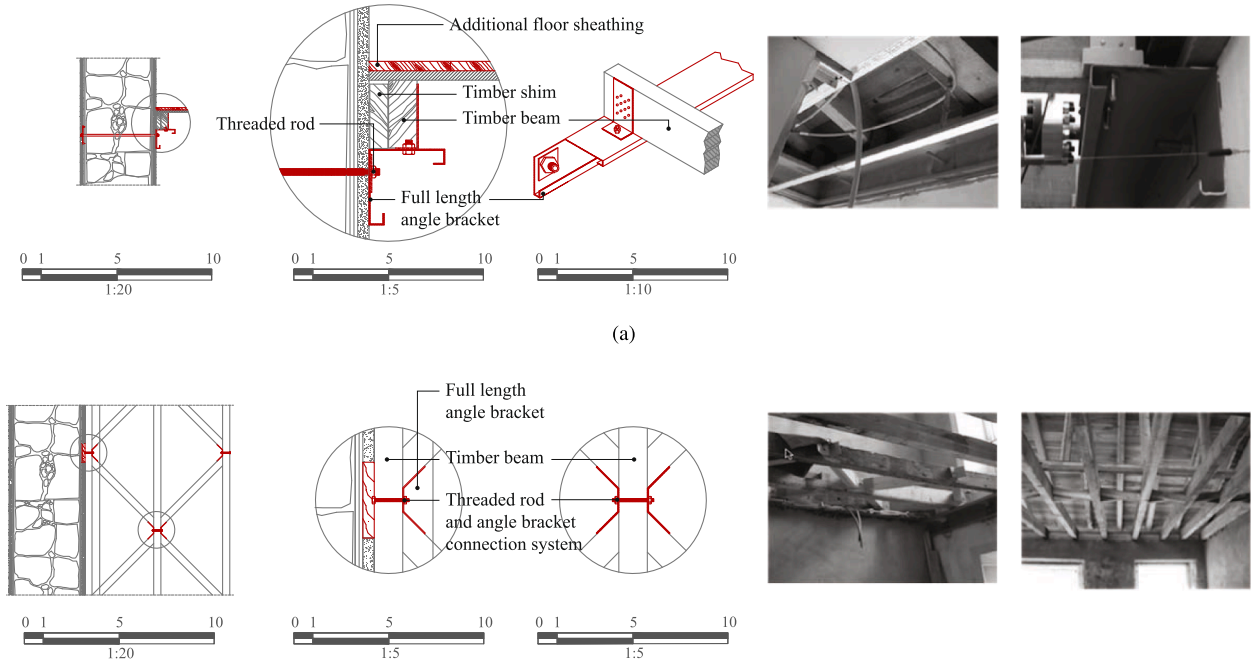

Fig. 5. Consolidation of the horizontal structure (2).

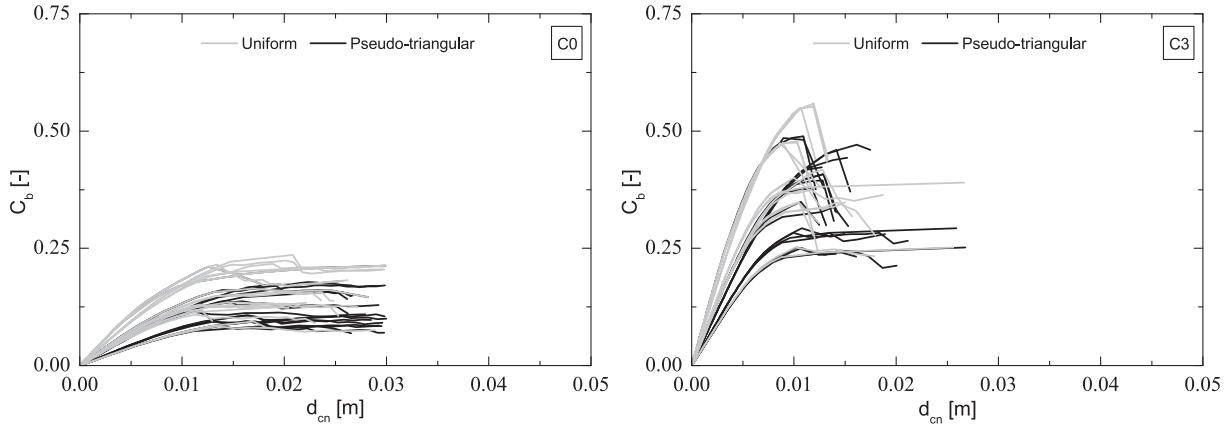

Fig. 6. Example of the pushover curves obtained for model C, grouped by horizontal load pattern distribution (uniform and pseudo-triangular), associated with the unreinforced condition (left) and the consolidation of both vertical and horizontal structures (right).

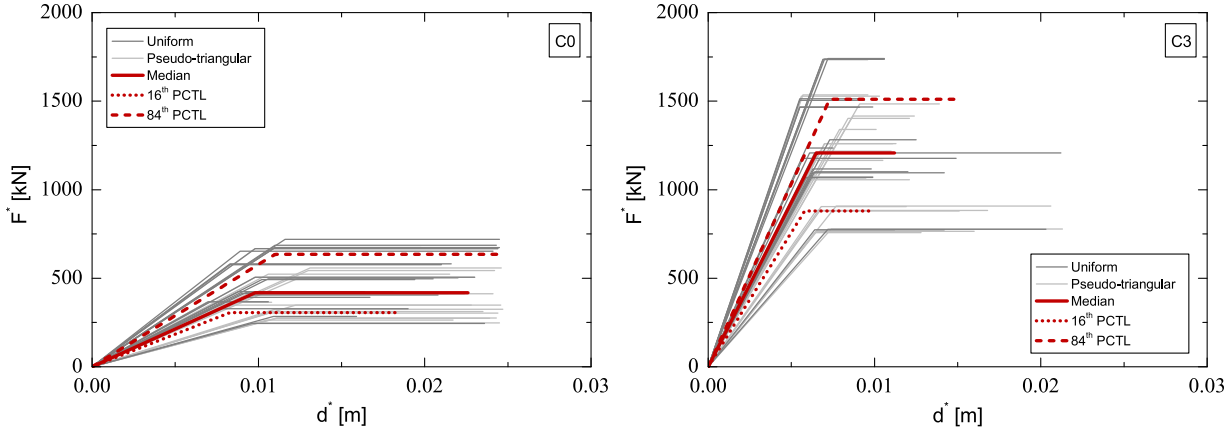

Fig. 7. Capacity curves obtained for model C, grouped by horizontal load pattern distribution (uniform and pseudo-triangular), associated with the unreinforced condition (left) and the consolidation of both vertical and horizontal structures (right).

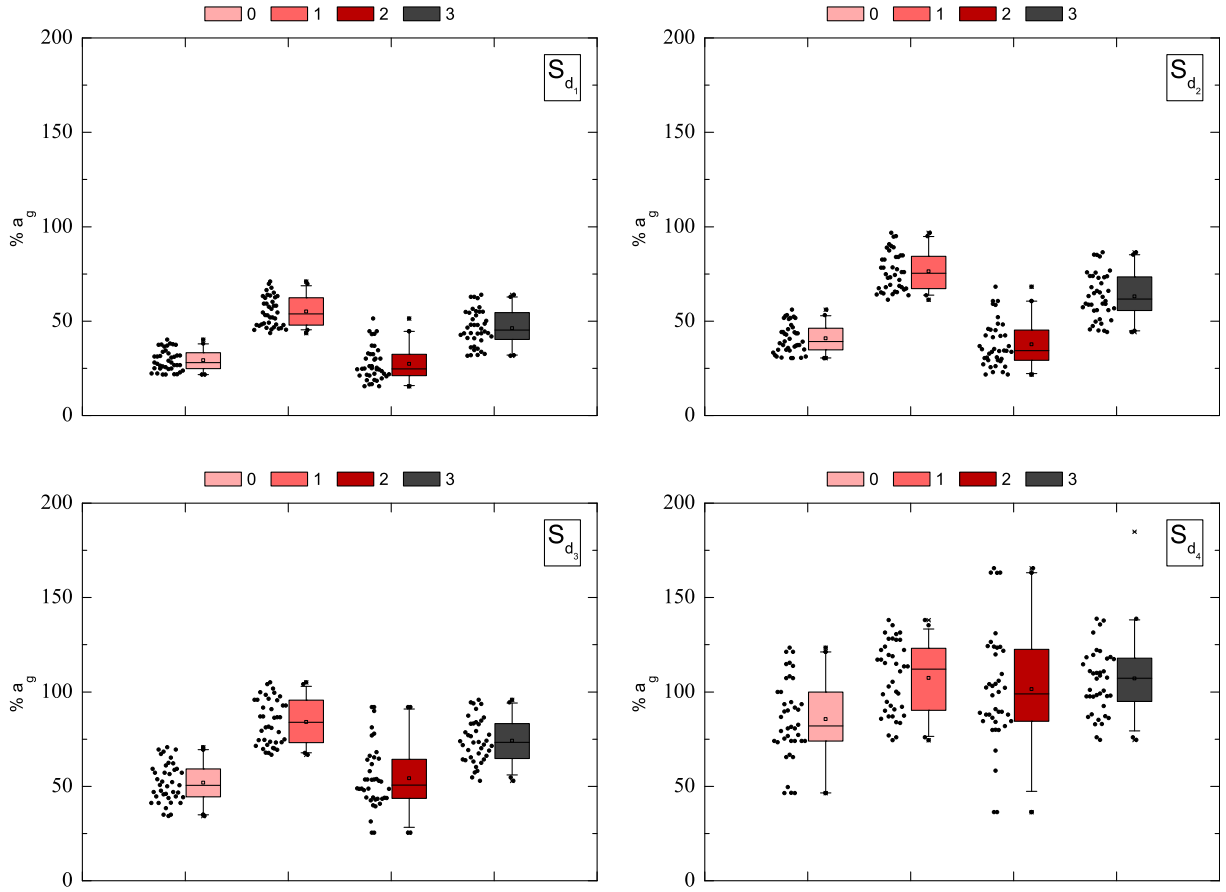

Fig. 8. Box-plot diagrams in terms of % a_g for the set of 40 pushover analyses performed for model C, grouped by limit state (from S_{d_1} to S_{d_4} and retrofitting condition (from 0 to 3).

application of retrofitting strategies 1 and 2 simultaneously.

3. Global seismic performance-based assessment

The seismic performance of the models described in Section 2, was evaluated according to the nonlinear static analysis procedure [28] recommended by the EN 1998-1 [26]. This procedure is commonly used to determine the structure's target displacement, $d*_t$, which is in turn computed from the intersection between the capacity spectrum of the structure (derived from the capacity curve) and the inelastic response spectrum associated with the demand in terms of seismic action, following the iterative procedure recommended in the NP EN 1998-1 [29]. Even though more sophisticated procedures are available, such as nonlinear dynamic incremental analysis, the N2 Method presents a good balance between precision in the estimation of the seismic performance of existing structures and computational effort. Moreover, such procedure is well suited to the simplicity of the numerical model herein used, which is based on the macroelement approach.

In this study, and for each model, a set of 40 pushover analyses was performed, 24 of which along different planar directions considering an incremental angular step of 30° and two different load pattern distributions (uniform, proportional to mass, and pseudo-triangular, proportional to the product between mass and height). The remaining 16 analyses were performed along the two main planar directions (X and Y) and by considering the accidental eccentricity as recommended by the NP EN 1998-1 [29]. This set of pushover curves, obtained for each model and retrofitting condition, represent the nonlinear relationship between the shear coefficient, C_b, and the displacement of the control node, d_{cn}. The shear coefficient C_b is obtained diving the base shear strength, V_b, by the total weight of each model, W. The following W values were obtained for each model from A to D: 1189.5 kN; 2108.3 kN; 3874.7 kN, and 11899.0 kN.

For the sake of an example, only the results referring to model C are going to be discussed in detail in this section. Hence, while the pushover curves in Fig. 6 (left) correspond to the unreinforced condition (0), the curves in Fig. 6 (right), correspond to the consolidation of both vertical and horizontal structures (3) of model C. Each set of curves is grouped in function of the type of load pattern distribution (uniform and pseudo-triangular), from were it is possible to observe that the uniform load pattern distribution reaches, in general, higher C_b values. From Fig. 6, it is also possible to observe a significant increase both in terms of base shear coefficient and initial stiffness with the application of retrofitting strategy 3. To the contrary, the ductility capacity of the retrofitting strategy 3 has decreased in comparison to the unreinforced condition (0). The pushover curves obtained for the remaining models are given in Appendix A.

The global displacement capacity of each model was evaluated by considering the damage limit state thresholds proposed by Barbat et al. [30], which are directly dependent on the values of the yielding and ultimate spectral displacement, S_{d_y} and S_{d_u}, respectively. The limit states from Eq. (1) to Eq. (4), refer to the slight damage, moderate damage, severe damage and collapse damage limit states.

As demonstrated in Eq. (1) to Eq. (4), limit states S_{d_2} and S_{d_4}, are, in fact, directly correlated to the Damage Limitation (DL) and Near Collapse (NC) limit states, which are recommended by the NP EN 1998-1 [29]. Hence, the global displacement capacity for the NC limit state was defined by the magnitude of the roof displacement at the point corresponding to a 20% decay of the maximum base shear strength, according to the EN 1998-3 [23]. In the case of the DL limit state, the displacement capacity was defined at the yielding point of the idealised

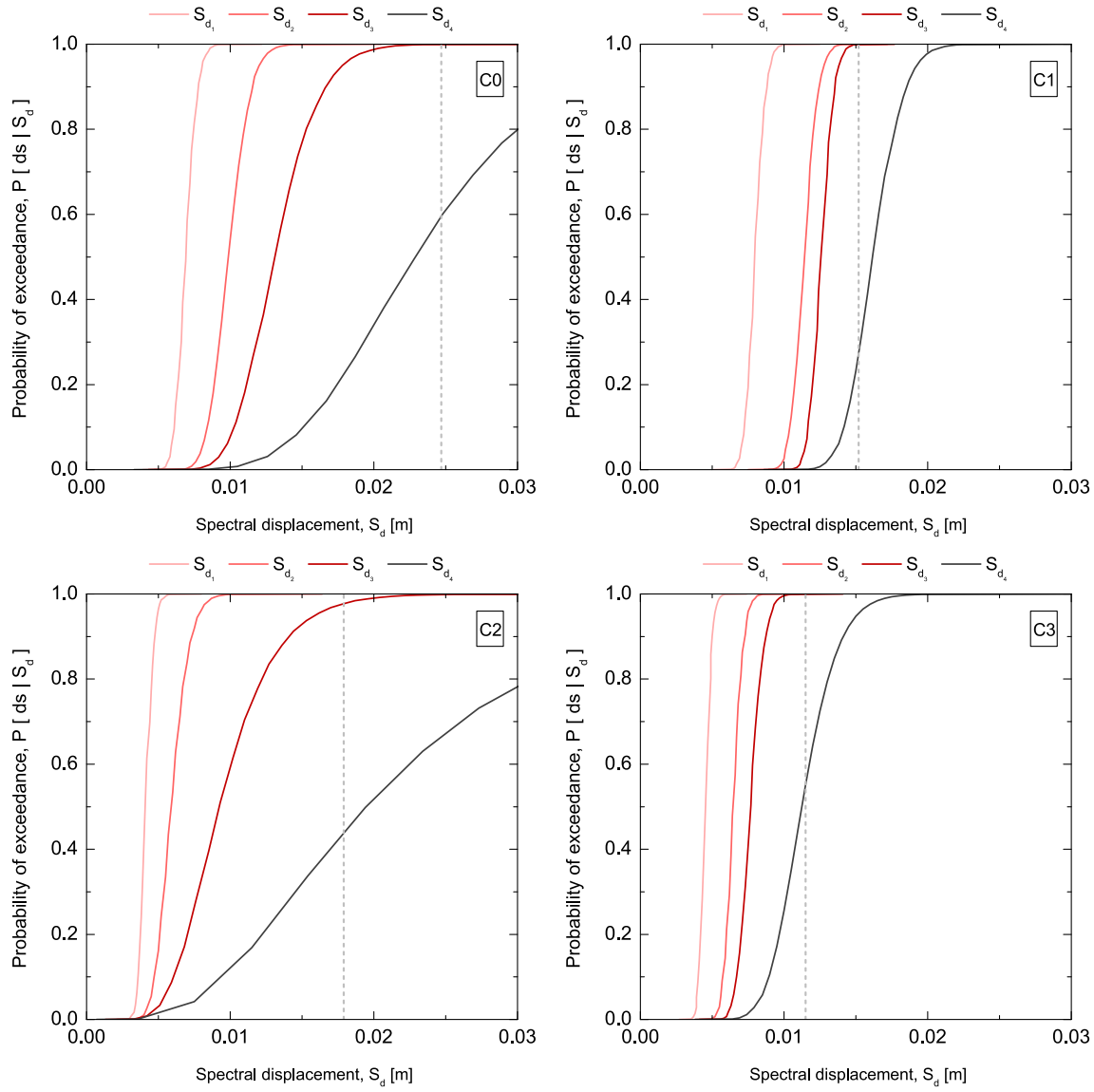

Fig. 9. Fragility curves associated with the median values of the capacity curves of model C, for each limit state (from S_{d_1} to S_{d_4} and retrofitting condition (from 0 to 3). Please note that the performance point of the equivalent bilinear SDoF system, $d*_t$, is represented for each case by the vertical dashed line in light grey.

elasto-plastic pushover curve. The control point for each model was selected at the rigidity centre of the horizontal diaphragms highlighted in Fig. 3 (at the roof level).

$$S_{d_1} = 0.7 \times S_{d_y} \quad (1)$$

$$S_{d_2} = DL = S_{d_y} \quad (2)$$

$$S_{d_3} = S_{d_2} + 0.25 \times (S_{d_u} - S_{d_y}) \quad (3)$$

$$S_{d_4} = NC = S_{d_u} \quad (4)$$

The capacity curves presented in Fig. 7, were obtained by applying a transformation coefficient [26,28] that allows converting the pushover curves (associated to the Multi Degree of Freedom system, MDoF) into an equivalent bilinear Single Degree of Freedom (SDoF) system, assuming an elasto-perfectly plastic force-displacement relationship. Fig. 7, also presents the capacity curves corresponding to the median, 16th and 84th percentiles (PCTL) of the set of the 40 analyses performed. These central tendency measures are going to be considered for the computation of fragility curves and subsequently on the cost-benefit analysis, as explained in Sections 4 and Sections 5, respectively.

Again, for the sake of an example, the capacity curves in Fig. 7, were derived from the pushover curves presented in the previous Fig. 6, being, for this reason, associated with the unreinforced condition (left) and consolidation of both vertical and horizontal structures (right) of model C. If focusing on the base shear strength of the equivalent bilinear SDoF system, F*, in Fig. 7 (left), the average values of 500 kN and 406 kN, were obtained for the analyses associated with the uniform and pseudo-triangular lateral load pattern distribution, respectively. On the contrary, in the case of Fig. 7 (right), which presents the capacity curves associated with the retrofitting strategy 3, the average F* values of 1301 kN and 1119 kN were estimated, respectively to the uniform and pseudo-triangular lateral load pattern distribution. The capacity curves obtained for the remaining models are provided in Appendix A.

Finally, the global seismic performance of these models and the respective retrofitting conditions, was evaluated by calculating the admissible peak ground acceleration (a_g), hereinafter represented by the percentage % a_g. This value was obtained by imposing to each of the above-mentioned limit states, the seismic displacement demand equal to the respective capacity. The seismic demand for the Azores region (zone 2.1 and horizontal elastic response spectrum of type 2) was defined for a reference ground acceleration, a_{gR}, equal to 2.50 ms^{-2}, as recommended by the National Annex of the NP EN 1998-1 [29]. These

Table 3
Probabilities of exceeding each damage state (from ds_0 to ds_4), for each model and retrofitting condition, here only for median values. The probabilities associated with the 16th and 84th PCTL are summarised in Appendix A.

Model	Retrofitting condition	ds_0	ds_1	ds_2	ds_3	ds_4
		No damage	Slight damage	Moderate damage	Severe damage	Collapse
A	0	0%	0%	0%	60%	40%
	1	80%	20%	0%	0%	0%
	2	0%	0%	0%	54%	46%
	3	93%	7%	0%	0%	0%
B	0	0%	0%	0%	35%	65%
	1	0%	12%	65%	22%	2%
	2	0%	0%	0%	34%	66%
	3	0%	20%	63%	16%	1%
C	0	0%	0%	0%	41%	59%
	1	0%	0%	0%	72%	28%
	2	0%	0%	2%	54%	44%
	3	0%	0%	0%	44%	56%
D	0	0%	0%	0%	6%	94%
	1	0%	0%	1%	70%	29%
	2	0%	0%	0%	42%	58%
	3	0%	0%	2%	68%	30%

Table 4
Global results of the cost-benefit analysis for each model and retrofitting condition (from 0 to 3), considering the median values and the traditional construction replacement cost, $C_{R,CT}$. The results associated with the 16th and 84th PCTL are summarised in Appendix A.

Model	Retrofitting condition	C_{RD}	C_{BC}	C_{HL}	Total losses	Benefit	BCR_{CT}
		€	€	€	€	€	[–]
A	0	53010	15894	1029	69932	–	–
	1	338	169	0	507	69425	8.11
	2	28861	17034	1187	47082	22850	14.20
	3	277	156	8	442	69491	6.83
B	0	69392	20286	6549	96227	–	–
	1	4094	3487	360	7941	88286	5.84
	2	50832	20473	6653	77958	18269	6.42
	3	3872	2862	299	7032	89195	4.96
C	0	127119	19358	4526	151002	–	–
	1	18378	13846	2233	34457	116546	3.70
	2	27599	16502	3405	47507	103496	17.49
	3	33868	18704	4253	56825	94177	2.52
D	0	246394	25443	9411	281248	–	–
	1	24826	13949	3074	41849	51069	3.38
	2	46099	19163	5933	71196	51837	18.22
	3	25633	14062	3177	42871	238377	3.27

values are recommended for structures with an importance class II, to which corresponds an importance factor, γ_I, equal to 1.00. In addition to the reference ground acceleration, the horizontal elastic response spectrum is fully characterised after the definition of the following parameters: $T_B = 0.10$ s; $T_C = 0.25$ s; $T_D = 2.0$ s; soil factor, S, equal to 1.30; equivalent viscous damping, ξ, equal to 5%, and foundation soil type C [29].

In this study three levels of the seismic action, associated to three different return periods, were considered, in accordance to the Portuguese National Annex of the EN 1998-3 [23]: 975 years for NC limit state; 308 years for the SD limit state, and 73 years for the DL limit state. This is the approach that it is currently in force in Portugal for retrofitting purposes.

The box-plot diagrams in terms of the % a_g values, obtained for model C, are presented in Fig. 8 for each limit state (from S_{d_1} to S_{d_4}) and retrofitting condition (from 0 to 3). It is possible to observe a greater dispersion on the results as one moves from limit state S_{d_1} to S_{d_4}. Another interesting observation, in the particular case of model C, is that the consolidation of the vertical structure (1) appears to substantially improve the median % a_g values for all the considered limit states, when compared to the unreinforced condition (0). To the contrary, the efficiency of the consolidation of the horizontal structure (2) is only observed in the case of limit state S_{d_4}. Moreover, from comparing the results in Fig. 8 it is possible to observe that retrofitting strategy 3 is far from representing a summation of the response obtained with retrofitting strategies 1 and 2 in terms of % a_g. Instead, if considering the median % a_g values, retrofitting strategy 3 is placed in an intermediate position between these two retrofitting strategies. This fact is observed for all limit states and for the great majority of the models herein considered, as demonstrated in Appendix A.

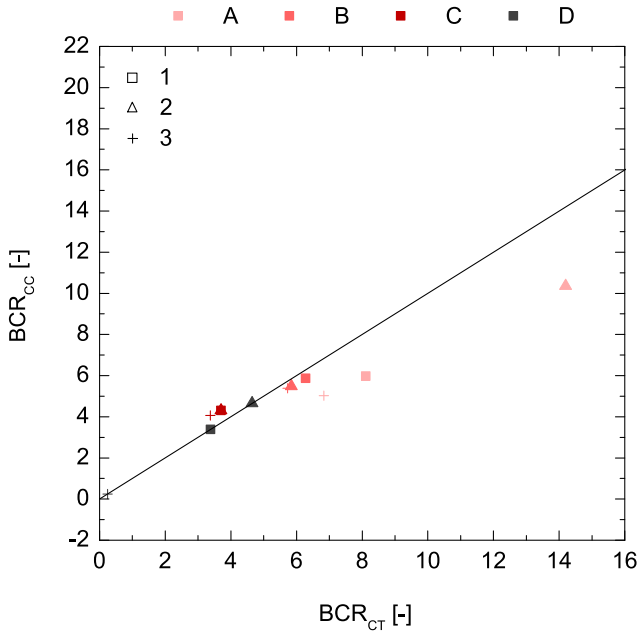

Fig. 10. Comparison between the median BCR_{CT} and BCR_{CC} ratios obtained for each model and retrofitting condition (from 1 to 3).

4. Fragility and loss assessment

In this study, the loss assessment was carried out by following the HAZUS methodology [31] for the computation of fragility curves, which represent the relationship between seismic intensity, herein expressed in terms of spectral displacement, and damage in terms of the conditional cumulative probability of reaching or exceeding a given damage state (ds). Hence, according to the HAZUS methodology [31], the following damage states should be considered: none damage (ds_0), slight damage (ds_1), moderate damage (ds_2), severe damage (ds_3), and complete damage or collapse (ds_4). The probability density function was assumed to follow a lognormal distribution [31]. Thus, the probability of a reaching or exceeding a given damage state, ds, is defined by Eq. (5), as a function of the spectral displacement, S_d:

$$P[ds|S_d] = \Phi\left[\frac{1}{\beta_{ds}} \times \ln\left(\frac{S_d}{\overline{S}_{d,ds}}\right)\right] \quad (5)$$

where Φ is the standard normal cumulative distribution function, β_{ds} is the standard deviation of the natural logarithm of the spectral displacement for the damage state ds, and $\overline{S}_{d,ds}$, is the median value of the spectral displacement at which a building reaches the threshold of damage state ds [31]. The standard deviation β_{ds}, which accounts for

the variability and uncertainty associated with the numerical model, capacity curve, seismic demand, and the definition of each damage states threshold, was computed according to the formulation proposed in the framework of the European project Risk-UE [32], given in Eq. (6) to Eq. (9). According to this formulation, the values of β_{ds} are closely related to the ultimate ductility of the structure, μ_u, defined as the ratio between d_u and d_y. Finally, the median values of the spectral displacement associated to each damage limit state, $\overline{S}_{d,ds}$, were adopted from Barbat et al. [30], according to the previous Eqs. (1)–(4).

$$\beta_{d_1} = 0.25 + 0.07 \times \ln(\mu_u) \quad (6)$$

$$\beta_{d_2} = 0.20 + 0.18 \times \ln(\mu_u) \quad (7)$$

$$\beta_{d_3} = 0.10 + 0.40 \times \ln(\mu_u) \quad (8)$$

$$\beta_{d_4} = 0.15 + 0.50 \times \ln(\mu_u) \quad (9)$$

Following the same reasoning as hitherto, and again for the sake of an example, the fragility curves in Fig. 9 are associated with the median capacity curves of each retrofitting condition of model C only. From observing these results, it is possible to conclude that the consolidation of the vertical structure (1) is in fact the most effective retrofitting strategy in this particular case, reducing the probability of reaching or exceeding the limit state S_{d_4} from 59% to 28%. In line with the results presented in Fig. 8, when comparing the consolidation of both vertical and horizontal structures simultaneously (3) with retrofitting strategies 1 and 2 individually, the probabilities of reaching or exceeding a given damage state (ds) are clearly exacerbated. In fact, in this particular case, the probabilities of exceeding each damage state for retrofitting strategy 3 are practically identical to the unreinforced condition (0). However, and as demonstrated in Appendix A, this abnormal outcome, which is highly influenced by the low displacement ductility capacity of model C when subject to retrofitting strategy 3, was not observed in the remaining models.

The computation of fragility curves is a necessary step to determine the probabilities p_k, of exceeding each damage state ds, and subsequently, apply the HAZUS loss assessment methodology [31]. These probabilities are summarised in Table 3 for each model, central tendency measure and retrofitting condition.

It is worth referring that the loss assessment in this study included the estimation of economic losses resulting from the need of repairing seismic-induced damage (RD), the damage caused to building contents (BC), and also from human casualties (HL), as detailed in the following subsections.

4.1. Repair damage (RD)

One of the most widely used approaches for the estimation of direct economic loss associated with a given damage level was included in the HAZUS methodology [31], through the seismic damage repair cost, C_{RD}, defined in Eq. (10):

$$C_{RD} = C_R \times \sum_{n=0}^{k} (f_{k,RD} \times p_k) \quad (10)$$

where C_R represents the replacement cost of the building, $f_{k,RD}$ the normalised deviation between the median C_{RD} values for each damage state (determined for the building stock of Faial Island by Maio et al. [1], and p_k, the probability of exceeding each one of these damage states (given in the previous Table 3). The $f_{k,RD}$ values of 0.000, 0.031, 0.059, 0.338, and 1.000 (respectively for damage states ds_0 to ds_4) were adopted from Maio et al. [1].

It is worth noting that two different values were considered for the building replacement cost, C_R. A first value, from now on referred to as current construction replacement cost, $C_{R,CC}$, was determined based on the average price for new construction, fixed by the Portuguese Ministerial Ordinance No. 330-A/2018 in 2019, in 492€/m^2 [33], to which a cost associated to demolition works was added. Thus, and after consulting average costs for demolition works in Portugal, the authors considered a final $C_{R,CC}$ value of 530€/m^2. A second value was considered to take into account the costs of reconstruction by preserving the original characteristics (traditional materials and building techniques) of the Faial Island vernacular architecture, from now on referred to as traditional construction replacement cost, $C_{R,CT}$. Such interventions were carried out during the reconstruction process of Faial Island after the 1998 Azores earthquake. The $C_{R,CT}$ values were derived from the curves proposed by Maio et al. [1], as a function of the GFA, and represent about 137%, 101%, 89% and 89% of the $C_{R,CC}$ value, respectively for model A to D. Hence, the resulting C_{RD} values are summarised further on, in Table 4 (Section 5).

4.2. Building contents (BC)

By building contents, the authors refer to the set of all movable assets present in a given building, from furniture and household appliances to increased value objects. These assets are particularly vulnerable to accelerations. For this reason, it's fundamental to consider damage to building contents in loss assessment procedures, even for low seismic intensity levels. The HAZUS methodology recommends that the losses associated with the replacement of building contents are determined as a function of the damage limit states of each building [31]. The reason why the authors have considered the recommendations of FEMA & NIBS [31] for the estimation of building contents loss had to due with the context where this study is inserted (more focused on urban-scale assessment) and to the fact that very little literature is available on this topic worldwide. Since the value of these buildings' contents is unknown, the replacement cost of the building contents, C_{BC}, was assumed equal to 50% of the repair cost C_R [31]. The replacement cost of the building contents, C_{BC}, are determined by means of Eq. (11). The $f_{k,BC}$ factors, which represent the normalised deviation between the median C_{BC} values for each damage limit state (from ds_0 to ds_4), were assigned equal to 0.000, 0.010, 0.050, 0.250, and 0.500, according to [31]. The resulting C_{BC} values are summarised further on, in Table 4 (Section 5).

$$C_{BC} = 0.5 \times C_R \times \sum_{n=0}^{k} (f_{k,BC} \times p_k) \quad (11)$$

4.3. Human loss (HL)

Human losses were also estimated according to the HAZUS methodology [31], again as a function of the damage limit states. According to this procedure, four severity levels are considered: injuries requiring basic medical aid, but without hospitalisation; injuries requiring medical attention and hospitalisation, but not considered to be life-threatening; casualties that include entrapment and require expeditious rescue and medical treatment to avoid death, and immediate deaths. The $f_{k,HL}$ factors associated with each severity level and damage limit state were adopted from FEMA & NIBS [31], considering the unreinforced masonry bearing walls typology (URM) and a scenario where the earthquake would occur at 2 a.m., i.e., residents were assumed to be inside their households.

The number of residents according to the information available in the inspection surveys carried out after the 1998 Azores earthquake was 1, 4, 3 and 4, respectively for building A to D. The percentage of injured residents was determined according to the values proposed in FEMA & NIBS [31] for residential buildings. The monetary values associated with each severity level were adopted from Lamego [34], which were derived in turn from the cost data analysis of the 1994 Northridge earthquake. The final costs associated with human loss, C_{HL}, are given in Table 4 (next section).

5. Cost-benefit analysis

The global outputs of the cost-benefit analysis carried out in this study, are summarised in the following Table 4, for each building and retrofitting strategy, considering only the median values and the $C_{R,CT}$ replacement cost. Economic losses are broken down in terms of repair damage (C_{RD}), building contents (C_{BC}), and human casualties (C_{HL}). The indicator BCR, represents the ratio between the gains obtained by preventing seismic-induced damage (Benefit), and the specific cost of each retrofitting strategy, C_{RS}. The cost of each retrofitting strategy, C_{RS}, was obtained by multiplying the average values proposed in Maio et al. [1] (equal to 117€/m^2, 22€/m^2, and 139€/m^2, respectively to retrofitting strategies 1 to 3) by the GFA of each case study building. When comparing the C_{RS} values with the $C_{R,CT}$ of each building, it is possible to observe that the cost of retrofitting strategies 1, 2, and 3, represent about 16%, 3%, and 19% of the $C_{R,CT}$ for model A, and 22%, 4%, and 26% for model B. For the urban typologies, the cost of retrofitting strategies 1, 2, and 3, represent about 25%, 5%, and 30% of $C_{R,CT}$ (practically the same for models C and D). If instead the $C_{R,CC}$ is to be compared with C_{RS}, one can conclude that retrofitting strategies 1, 2, and 3, represent 22%, 4%, and 26% of $C_{R,CC}$, independently from the building in question.

From analysing the final costs estimated by following the HAZUS methodology assuming the traditional construction replacement cost, $C_{R,CT}$ (in Table 4), the costs associated with human losses, C_{HL}, clearly stand out among the remaining ones (C_{RD} and C_{BC}). In fact, the relatively low values obtained for C_{HL} are closely related to the extremely low number of residents considered for each building.

When analysing the benefit column in Table 4, which represents the gains obtained by preventing seismic-induced damage with the application of each retrofitting strategies, it is possible to observe that, in the case of rural typologies (models A and B), greater economic gains are associated with retrofitting strategies 1 and 3. In the case of urban typologies (models C and D), retrofitting strategies 1 and 2 appear to have a more similar impact in terms of economic gains. However, if looking at the BCR_{CT} indicator in isolation, the consolidation of the horizontal structure (2) presents the highest benefit-cost ratios for the majority of the cases, due to the fact its application cost is significantly lower than the remaining strategies. Despite the BCR_{CT} indicator suggests the consolidation of the horizontal structure (2) as the most viable retrofitting strategy, this strategy appears to be, in fact, the less efficient in terms of seismic damage prevention, as previously suggested by the results presented in Table 3. The authors believe that this fact might be related to the compatibility issues between the definition of horizontal diaphragms within the software code used and the recommendations of the NZSEE guidelines [24].

In the following Fig. 10, the benefit-cost ratios obtained for both traditional and current construction replacement costs (BCR_{CT} and BCR_{CC}, respectively) are opposed for each building and retrofitting strategy. For the sake of simplicity, only the median values are presented in Fig. 10. It is possible to conclude that the benefit-cost ratios obtained by implementing traditional seismic retrofitting strategies when adopting replacement costs associated with a reconstruction process that makes use of the traditional construction techniques and materials, BCR_{CT}, are in fact higher than those associated with current construction replacement costs, BCR_{CC}, exception made to model C. In the case of model D, since the replacement costs $C_{R,CT}$ and $C_{R,CC}$ are practically equal, the resulting BCR_{CT} and BCR_{CC} ratios are identical.

6. Final remarks

This study aimed at outlining and testing a CBA model for evaluating the cost-benefit from integrating traditional seismic retrofitting strategies on the renovation of both rural and urban typologies of the vernacular architecture of Faial Island, in Azores (Portugal).

One of the first conclusions of this study is that, in general, the use of the seismic retrofitting strategies herein studied allows indeed, the improvement of the seismic performance of such building typologies. Furthermore, this study demonstrated that the cost of application of traditional retrofitting strategies does not embody a significant amount over the total replacement cost, that could possibly turn the use of these strategies economically unviable. Another interesting observation has to do with the large dispersion of the results, as a consequence of considering aspects such as the type of lateral load pattern distribution (uniform and pseudo-triangular), accidental eccentricity, loading directions, for example, in the analyses.

For the great majority of the cases analysed, the use of traditional seismic retrofitting strategies show a quite satisfactory benefit-cost ratio, being for this reason recommendable for both rural and urban building stock of Faial Island. In particular, the consolidation of the horizontal structure has proved to be the most attractive strategy for all the case studies if exclusively focusing on the benefit-to-cost ratio. However, and unexpectedly, this attractiveness is not echoed in terms of seismic performance upgrading. This fact broaches the subject of how the formulation of horizontal diaphragms in this type of software codes should be revised or adapted in order to enhance the compatibility between numerical models and the values recommended by the NZSEE guidelines for flexible diaphragms. In this regard, and as further developments, the improvement of the connections between horizontal diaphragms and load-bearing walls should be numerically investigated in detail so that the seismic performance upgrading in the numerical models can be more approximated to the expected contribution of such retrofitting strategy.

Finally, it is worth referring that, since the replacement costs associated with the use of traditional materials and building techniques are in general lower than those associated with current construction, higher benefit-cost ratios are obtained. This finding constitutes, therefore, a great incentive for promoting the proper renovation of UCH assets in Faial Island.

Declaration of Competing Interest

The authors declare that they have no known competing financial interests or personal relationships that could have appeared to influence the work reported in this paper.

Acknowledgements

This study was supported by the Foundation for Science and Technology (FCT) in the framework of the doctoral programme Infrarisk- Analysis and Mitigation of Risks in Infrastructures (PD/BD/128100/2016). The authors acknowledge to the Society of Promotion for Housing and Infrastructures Rehabilitation (SPRHI) and Regional Secretariat for Housing and Equipment (SRHE), and in particular to Professors Aníbal Costa and Carlos Sousa Oliveira for having made available the database of the reconstruction process of the Faial Island. Moreover, the authors would like to thank the team of Gruppo Sismica, in particular to Dr. Bartolomeo Pantò, Dr. Sandro Liseni and Dr. Davide Rapicavoli, for their support with 3D-Macro® software code.

Appendix A

See Figs. 11–14 and Tables 5 and 6.

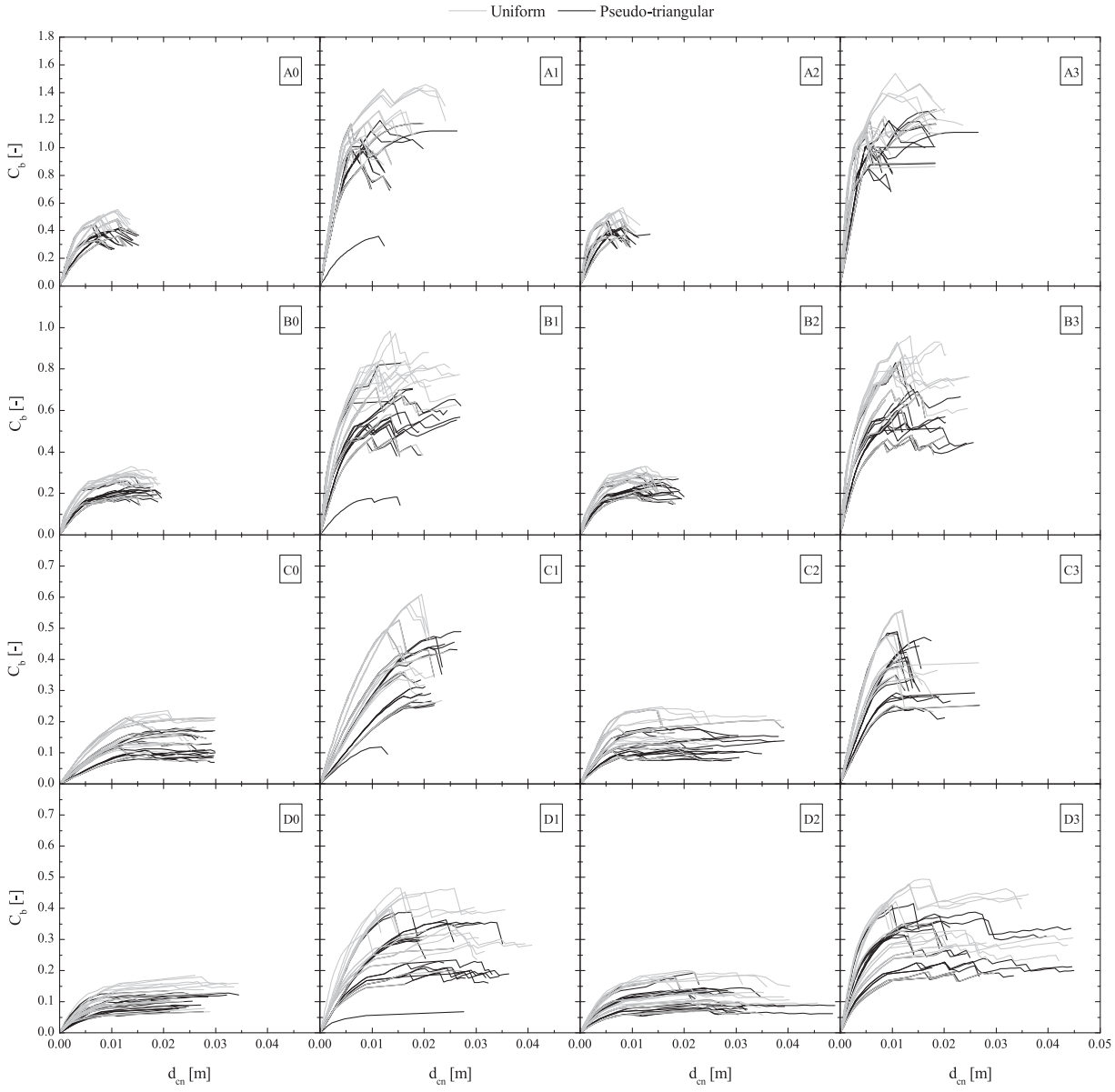

Fig. 11. Pushover curves obtained for each model (from A to D) and retrofitting condition (from 0 to 3) and grouped by horizontal load pattern distribution (uniform and pseudo-triangular).

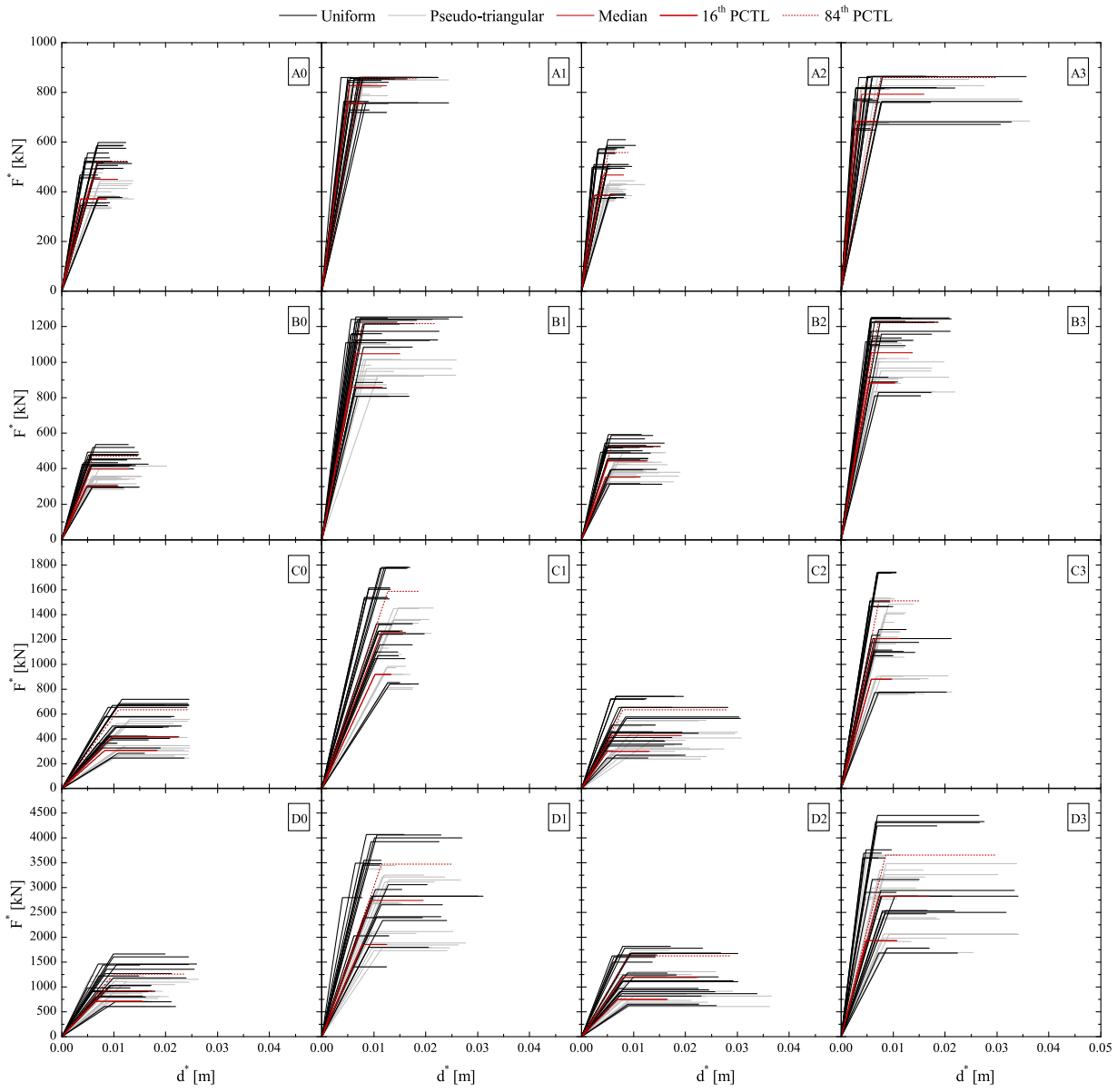

Fig. 12. Capacity curves obtained for each model (from A to D) and retrofitting condition (from 0 to 3) and grouped by horizontal load pattern distribution (uniform and pseudo-triangular).

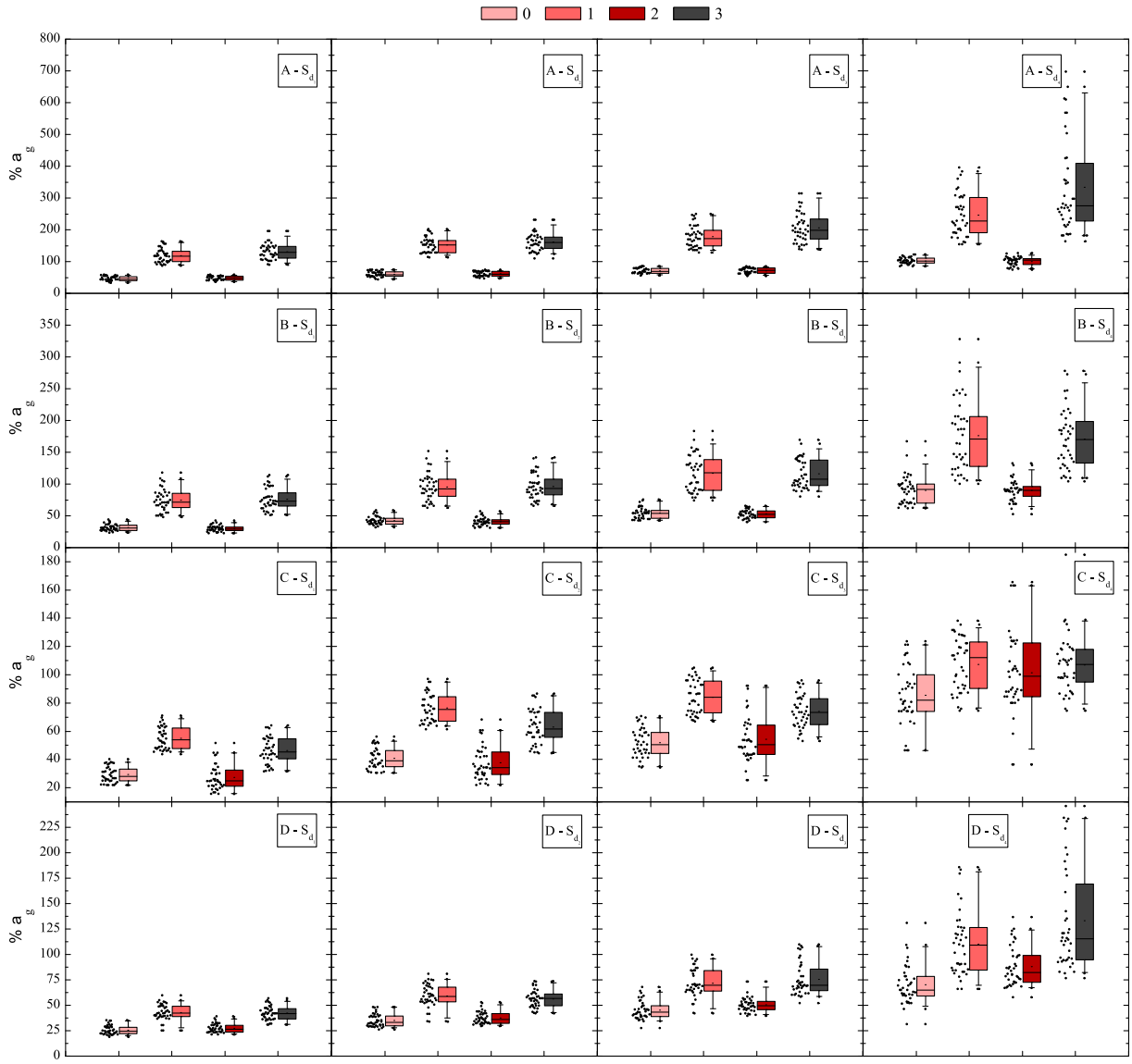

Fig. 13. Box-plot diagrams in terms of % a_g for the set of 40 pushover analyses performed for each model (from A to D) and retrofitting condition (from 0 to 3) and grouped by limit state (from S_{d_1} to S_{d_4}).

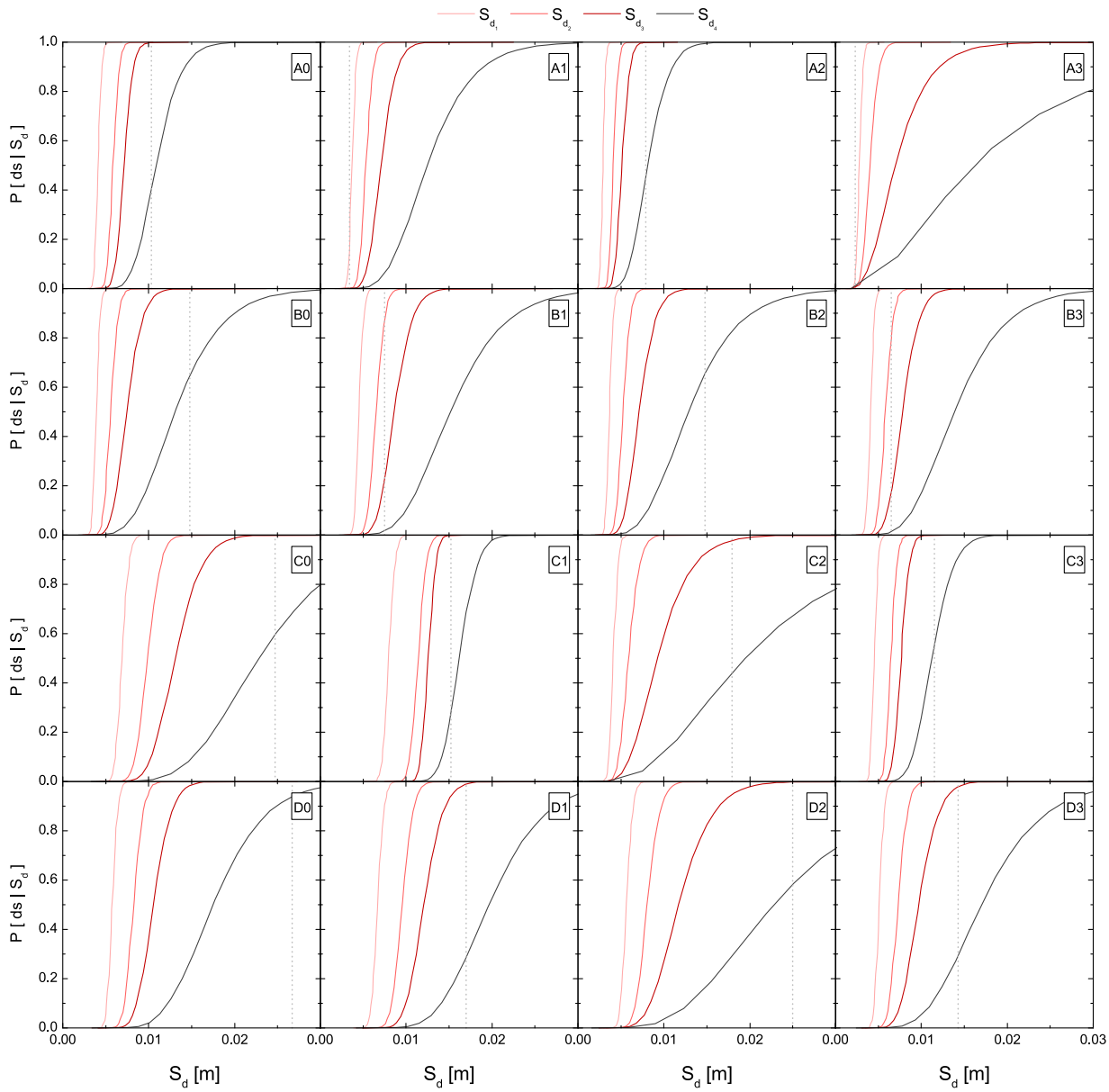

Fig. 14. Fragility curves associated with the median values of the capacity curves for each model (from A to D) and retrofitting condition (from 0 to 3). Please note that the performance point of the equivalent bilinear SDoF system, $d*_t$, is represented for each case by the vertical dashed line in light grey.

Table 5
Probabilities of exceeding each damage state (from ds_0 to ds_4), for each model (from A to D) and retrofitting condition, considering the median values.

Building	Central tendency measure	Retrofitting condition	ds_0 No damage	ds_1 Slight damage	ds_2 Moderate damage	ds_3 Severe damage	ds_4 Collapse
A	Median	0	0%	0%	0%	60%	40%
		1	80%	20%	0%	0%	0%
		2	0%	0%	0%	54%	46%
		3	93%	7%	0%	0%	0%
	16th PCTL	0	0%	0%	1%	59%	41%
		1	99%	1%	0%	0%	0%
		2	0%	0%	2%	59%	39%
		3	99%	1%	0%	0%	0%
	84th PCTL	0	0%	0%	1%	44%	56%
		1	100%	0%	0%	0%	0%
		2	0%	0%	0%	17%	83%
		3	100%	0%	0%	0%	0%

(*continued on next page*)

Table 5 (*continued*)

Building	Central tendency measure	Retrofitting condition	ds_0 No damage	ds_1 Slight damage	ds_2 Moderate damage	ds_3 Severe damage	ds_4 Collapse
B	Median	0	0%	0%	0%	35%	65%
		1	0%	12%	65%	22%	2%
		2	0%	0%	0%	34%	66%
		3	0%	20%	63%	16%	1%
	16th PCTL	0	0%	0%	0%	27%	73%
		1	0%	87%	12%	1%	0%
		2	0%	0%	0%	33%	67%
		3	4%	93%	2%	0%	0%
	84th PCTL	0	0%	0%	0%	35%	65%
		1	0%	8%	66%	23%	3%
		2	0%	0%	0%	43%	57%
		3	0%	5%	64%	28%	3%
C	Median	0	0%	0%	0%	41%	59%
		1	0%	0%	0%	72%	28%
		2	0%	0%	2%	54%	44%
		3	0%	0%	0%	44%	56%
	16th PCTL	0	0%	0%	0%	32%	68%
		1	0%	0%	0%	70%	30%
		2	0%	0%	0%	32%	68%
		3	0%	0%	1%	77%	22%
	84th PCTL	0	0%	0%	0%	20%	80%
		1	0%	0%	0%	53%	47%
		2	0%	0%	6%	58%	35%
		3	0%	0%	0%	58%	42%
D	Median	0	0%	0%	0%	6%	94%
		1	0%	0%	1%	70%	29%
		2	0%	0%	0%	42%	58%
		3	0%	0%	2%	68%	30%
	16th PCTL	0	0%	0%	0%	14%	86%
		1	0%	0%	0%	22%	78%
		2	0%	0%	0%	26%	74%
		3	0%	0%	0%	50%	49%
	84th PCTL	0	0%	0%	0%	19%	81%
		1	0%	0%	5%	75%	20%
		2	0%	0%	0%	42%	57%
		3	0%	0%	21%	59%	20%

Table 6
Global results of the cost-benefit analysis for each model (from A to D), central tendency measure, and retrofitting condition (from 0 to 3), considering the traditional construction replacement cost, $C_{R,CT}$.

Building	Central tendency measure	Retrofitting condition	C_{RD} €	C_{BC} €	C_{HL} €	Total losses €	Benefit €	BCR_{CT} [–]
A	Median	0	53010	15894	1029	69932	–	–
		1	338	169	0	507	69425	8.11
		2	28861	17034	1187	47082	22850	14.20
		3	277	156	8	442	69491	6.83
	16th PCTL	0	53010	16043	1055	70108	–	–
		1	16	8	0	24	70083	8.19
		2	24875	15672	1015	41563	28545	17.74
		3	12	6	0	19	70089	6.89
	84th PCTL	0	53010	18841	1437	73287	–	–
		1	3	2	0	5	73282	8.56
		2	46630	23566	2092	72289	998	0.62
		3	34	15	0	48	73239	7.20

(*continued on next page*)

Table 6 (*continued*)

Building	Central tendency measure	Retrofitting condition	C_{RD} €	C_{BC} €	C_{HL} €	Total losses €	Benefit €	BCR_{CT} [–]
B	Median	0	69392	20286	6549	96227	–	–
		1	4094	3487	360	7941	88286	5.84
		2	50832	20473	6653	77958	18269	6.42
		3	3872	2862	299	7032	89195	4.96
	16th PCTL	0	69392	21700	7333	98425	–	–
		1	2394	986	36	3417	95008	6.28
		2	51616	20696	6777	79090	19335	6.80
		3	2104	812	8	2923	95501	5.31
	84th PCTL	0	69392	20314	6565	96270	–	–
		1	5076	3924	500	9500	86770	5.73
		2	45017	18876	5773	69666	26605	9.35
		3	4959	4311	508	9778	86492	4.81
C	Median	0	127119	19358	4526	151002	–	–
		1	18378	13846	2233	34457	116546	3.70
		2	27599	16502	3405	47507	103496	17.49
		3	33868	18704	4253	56825	94177	2.52
	16th PCTL	0	127119	20890	5163	153171	–	–
		1	19890	14287	2415	36592	116580	3.70
		2	39899	20872	5156	65927	87244	14.74
		3	14633	12742	1792	29167	124004	3.32
	84th PCTL	0	127119	23009	6045	156173	–	–
		1	29408	17215	3633	50256	105916	3.37
		2	22661	14705	2780	40147	116026	19.61
		3	26592	16305	3260	46157	110016	2.94
D	Median	0	246394	25443	9411	281248	–	–
		1	24826	13949	3074	41849	51069	3.38
		2	46099	19163	5933	71196	51837	18.22
		3	25633	14062	3177	42871	238377	3.27
	16th PCTL	0	246394	23981	8599	278975	–	–
		1	58191	22657	7865	88712	70289	4.65
		2	55614	21868	7427	84909	42357	14.89
		3	40124	17614	5072	62810	216164	2.97
	84th PCTL	0	246394	23125	8124	277643	–	–
		1	17660	12135	2215	32011	3698	0.24
		2	45364	18956	5828	70148	40612	14.27
		3	0	10951	2224	13175	264468	3.63

Appendix B. Supplementary material

Supplementary data associated with this article can be found, in the online version, at https://doi.org/10.1016/j.engstruct.2019.110050.

References

[1] R. Maio, T. Ferreira, R. Vicente, A. Costa, Is the use of traditional seismic strengthening strategies economically attractive in the renovation of urban cultural heritage assets in Portugal?, Bulletin of Earthquake Engineering 10. doi:10.1007/s10518-018-00527-7.

[2] Oliveira C, Costa A, Nunes J. Sismo 1998 Açores – Uma década depois. Portugal: Maia; 2008.

[3] FEMA-255. Seismic rehabilitation of federal buildings: A benefit/cost model – Volume 1: A user's manual. Tech Rep., Federal Emergency Management Agency, Washington DC, United States of America; 1994.

[4] FEMA-256. Seismic rehabilitation of federal buildings: A benefit/cost model – Volume 2: Support documentation. Tech. Rep., Federal Emergency Management Agency, Washington DC, United States of America; 1994.

[5] Kappos A, Pitilakis K, Stylianidis K, Morfidis K, Asimakopoulos N. Cost-benefit analysis for the seismic rehabilitation of buildings in Thessaloniki, based on a hybrid method of vulnerability assessment. 5th International Conference on Seismic Zonation, Nice, France, October 17–19. 1995.

[6] Kappos A, Dimitrakopoulos E. Feasibility of pre-earthquake strengthening of buildings based on cost-benefit and life-cycle cost analysis, with the aid of fragility curves. Nat Hazards 1995;45:33–54. https://doi.org/10.1007/s11069-007-9155-9.

[7] Liel A, Deierlein G. Cost-benefit evaluation of seismic risk mitigation alternatives for older concrete frame buildings. Earthq Spectra 2013;29(4):1391–411. https://doi.org/10.1193/030911EQS040M.

[8] Marques R, Lamego P, Lourenço P, Sousa M. Efficiency and cost-benefit analysis of seismic strengthening techniques for old residential buildings in Lisbon. J Earthq Eng 2017. https://doi.org/10.1080/13632469.2017.1286616.

[9] Chrysostomou C, Kyriakides N, Papanikolaou V, Kappos A, Dimitrakopoulos E, Giouvanidis A. Vulnerability assessment and feasibility analysis of seismic strengthening of school buildings. Bull Earthq Eng 2015;13(12):3809–40. https://doi.org/10.1007/s10518-015-9791-5.

[10] Jaimes M, Niño M. Cost-benefit analysis to assess seismic mitigation options in Mexican public school buildings. Bull Earthq Eng 2017;15(9):3919–42. https://doi.org/10.1007/s10518-017-0119-5.

[11] Bento R, Lopes M, R C. Seismic evaluation of old masonry buildings. Part II: analysis of strengthening solutions for a case study. Eng Struct 2005;27(14):2014–23. https://doi.org/10.1016/j.engstruct.2005.06.011.

[12] Costa A, Arêde A. Strengthening of structures damaged by the Azores earthquake of 1998. Constr Build Mater 2006;20(4):252–68. https://doi.org/10.1016/j.conbuildmat.2005.08.029.

[13] Branco M, Guerreiro L. Seismic rehabilitation of historical masonry buildings. Eng Struct 2011;33(5):1626–34. https://doi.org/10.1016/j.engstruct.2011.01.033.

[14] Scotta R, Trutalli D, Marchi L, Pozza L. Seismic response of masonry buildings with alternative techniques for in-plane strengthening of timber floors. Revista Portuguesa de Engenharia de Estruturas 2017;3(4):47–58.

[15] Diz S, Costa A, Costa A. Efficiency of strengthening techniques assessed for existing masonry buildings. Eng Struct 2015;101:205–15. https://doi.org/10.1016/j.engstruct.2015.07.017.

[16] Moreira S. Seismic retrofit of masonry-to-timber connections in historical constructions Ph.D. thesis School of Engineering, University of Minho; 2015.

[17] Maio R, Estêvão J, Ferreira T, Vicente R. The seismic performance of stone masonry buildings in Faial island and the relevance of implementing effective seismic strengthening policies. Eng Struct 2017;141(2017):41–58. https://doi.org/10.1016/j.engstruct.2017.03.009.

[18] Ortega J. Seismic vulnerability of vernacular architecture Ph.D. thesis School of

Engineering, University of Minho; 2018.
[19] Costa A. Determination of mechanical properties of traditional masonry walls in dwellings of Faial Island, Azores. Earthq Eng Struct Dynam 2002;31(February 2000):1361–82. https://doi.org/10.1002/eqe.167.
[20] Pantò B, Cannizzaro F, Caliò I, Lourenço P. Numerical and experimental validation of a 3D macro-model for the in-plane and out- of-plane behaviour of unreinforced masonry walls. Int J Archit Heritage 2017;11(7):946–64. https://doi.org/10.1080/15583058.2017.1325539%0A.
[21] 3D-Macro. Il software per le murature (3d computer program for the seismic assessment of masonry buildings) – Release 4.1.2. Tech. Rep., Gruppo Sismica s.r.l., Catania, Italy; 2017.
[22] NTC. Decreto Ministeriale 14/1/2008 – Norme tecniche per le costruzioni. Tech. Rep. Gazzetta Ufficiale S.O. n.30 on 4/2/2008, Ministry of Infrastructures and Transportations; 2017.
[23] NP EN 1998-3. Eurocódigo 8: Projecto de estruturas para resistência aos sismos – Parte 3: avaliação e reabilitação de edifícios. Tech. Rep., European Committee for Standardization (CEN); 2017.
[24] Assessment and improvement of the structural performance of buildings in earthquake. recommendations of a NZSEE study group Tech. Rep., New Zealand. Wellington, New: Society for Earthquake EngineeringZealand; 2015.
[25] ASCE. Seismic evaluation and retrofitting of existing buildings. Tech. Rep. ASCE 41-13, American Society of Civil Engineers, Reston, Virginia, United States of America; 2017.
[26] EN 1998–1. Eurocode 8: design of structures for earthquake resistance – Part 1: general rules, seismic actions and rules for buildings. Tech. Rep., European Committee for Standardization (CEN), Brussels, Belgium; 2004.
[27] Braga A, Estêvão J. Feasibility of confined masonry design in Azores, in. Proceedings of the Azores 1998 - International Seminar on Seismic Risk and Rehabilitation of Stone Masonry Housing, Azores, Portugal. 2008. p. 1–10.
[28] Fajfar P. Gašperšič, The N2 method for the seismic damage analysis of RC buildings. Earthq Eng Struct Dyn 1996;25(1):31–46. https://doi.org/10.1002/(SICI)1096-9845(199601)25:1<31::AID-EQE534>3.0.CO;2-V.
[29] NP EN 1998–1. Eurocódigo 8: Projecto de estruturas para resistência aos sismos – Parte 1: regras gerais, acções sísmicas e regras para edifícios. Tech. Rep., European Committee for Standardization (CEN); 2009.
[30] Barbat A, Pujades L, Lantada N. Seismic damage evaluation in urban areas using the capacity spectrum method: Application to Barcelona. Soil Dyn Earthq Eng 2008;28(10–11):851–65. https://doi.org/10.1016/j.soildyn.2007.10.006.
[31] FEMA & NIBS. Multi-hazard loss estimation methodology: earthquake model, HAZUS-MH MR4. Tech. Rep., Federal Emergency Management, Mitigation Division, Washington, United States of America; 2003.
[32] Mouroux P, Le Brun B. Presentation of RISK-UE project. Bull Earthq Eng 2006;4(4):323–39. https://doi.org/10.1007/s10518-006-9020-3.
[33] Portugal. Portaria no. 330-A/2018 de 20 de dezembro de 2018. portaria que fixa o valor médio de construção por metro quadrado. Tech. Rep., Diário da República n. 245/2018, 1. Suplemento, Série I de 2018-12-20; 2015.
[34] Lamego P. Seismic Strengthening of Residential Buildings. Risk Analysis and Mitigation Ph.D. thesis School of Engineering, University of Minho; 2014.